Jurnal Polimesin
Department of Mechanical Engineering
State Polytechnic of Lhokseumawe
http://e-jurnal.pnl.ac.id/polimesin
e-ISSN : 2549-1999 No. : 4 Month : August
p-ISSN : 1693-5462 Volume : 22 Year : 2024

Article Processing Dates: Received on 2024-01-17, Reviewed on 2024-02-27, Revised on 2024-06-26, Accepted on 2024-07-03 and Available online on 2024-08-30

Drive system selection and the development of chassis structure basic design for medium-sized urban electric bus

Naufal Aflah Hibatullah[1] and Rachman Setiawan[2*]
[1]Master Degree Program of Mechanical Engineering Department, Institut Teknologi Bandung, Bandung, 40132, Indonesia
[2]Faculty of Mechanical and Aerospace Engineering, Institut Teknologi Bandung, Bandung, 40132, Indonesia
*Corresponding author: r.setiawan@itb.ac.id

Abstract

One of the alternative solutions to address environmental and energy challenges is the utilization of electric vehicles, particularly in the domain of public transportation. The focus was on the development of medium-sized electric buses to expand the reach of electric-powered public transport. The design process encompasses the selection of vehicle components, such as the drive system, and the configuration of a space frame chassis structure. The drive system was meticulously chosen and proved to exceed the design requirements, as it achieved a gradability of 12.44%, surpassing the targeted capability of 10% slope. Moreover, it boasts a maximum speed of 108 km/h, exceeding the design requirement of a maximum speed of 50 km/h, and can accelerate at a rate of 1-2 m/s². The chassis design adheres to regulations and standards and is grounded in the strength, stiffness, and natural frequency criteria. The initial chassis design did not meet the design requirement, however, through several iterations, a chassis structure was achieved with a vertical bending stiffness of 8.57 kN/mm and a torsional stiffness of 9.63 kNm/°. Based on the outcomes of this research, a drive system and chassis structure design that fully satisfies all the existing design requirements has been successfully attained.

Keywords:
Medium-sized electric bus, urban application, design process, drive system, chassis structure.

1 Introduction

Electric vehicles are an alternative to overcome environmental and energy problems because electric vehicles tend to produce lower emissions and have better energy efficiency when compared to fossil fuel vehicles, particularly mass transport, which has a noteworthy difference [1-3]. In Indonesia, the use of electric vehicles as a mode of transportation still tends to be limited to rail-based vehicles such as *Kereta Rel Listrik* (KRL), Mass Rapid Transit (MRT), and *Lintas Raya Terpadu* (LRT). For ground vehicles, there are large electric buses on specific routes [4, 5]. Hence, several urban areas still need to be covered by electric public transport, so utilizing a medium-sized electric bus is of interest to increase the reach of electric public transport and solve the congestion problem in urban areas.

Currently, the available medium-sized electric buses do not meet Indonesian regulations. Their Gross Vehicle Weight (GVW) typically ranges from 8,400 kg to 14,500 kg, exceeding the 8,000 kg GVW limit set by the Ministry of Transportation Regulation [6-11]. Therefore, there is a need to develop electric buses that comply with existing regulations.

Based on the product architecture, the electric bus consists of various main systems and components, such as the drive system and chassis structure, which is the main focus of this study.

The design of a drive system is constrained by the motion behavior and performance requirements of the vehicle. Vehicle motion analysis determines the drag forces (aerodynamic, road gradient, rolling resistance, and acceleration) acting on the vehicle, which dictate the required traction force from the powertrain system [12, 13].

Powertrain selection comprehensively evaluates various factors, including torque, rotational speed, power generation, and power transmission [12, 13]. While numerous combinations can meet the specified criteria, over-design should be avoided. Therefore, the chosen powertrain components should deliver a system that exceeds the minimum requirements but remains as close to them as possible.

For medium buses, the chassis structure is typically divided into a space frame and ladder frame. Ladder frames, which are characterized by their longitudinal rails and transverse beams, offer straightforward manufacturing, modification, and repair advantages. Conversely, space frames, with their three-dimensional network of hollow metal, prioritise weight reduction and passenger space optimisation. This is achieved through their design flexibility, which allows for lower floor clearance and a larger passenger compartment. As regulations increasingly emphasize lightweight design, space frames gain favour due to their inherent weight savings [14, 15].

Several studies have explored chassis structures for buses that can be applied to medium-sized electric bus designs. For example, Gawande et al. achieved significant stiffness gains by optimising cross-member design [16], while Afzal et al. identified hexagonal hollow sections as particularly effective in enhancing torsional and bending stiffness [17]. Material substitution with aluminium alloys offers weight reduction benefits, as explored by Nandhakumar et al. [18], while Alifio et al. investigated even lighter materials such as magnesium and titanium; however, safety considerations limited the practical application of some lightweight options [19]. Satrijo et al. explored optimizing chassis mass through profile thickness modifications without compromising safety, achieving a mass reduction while maintaining structural integrity [20]. Wicaksono et al. utilized rollover tests to assess crashworthiness [21], and Arteaga et al. employed simulations based on established safety standards [22]. This study provides a valuable basis for development of a medium-sized electric bus chassis.

While designing a drive system and chassis structure for a medium-sized electric bus requires addressing limitations through Finite Element Analysis (FEA) for strength, stiffness, and crashworthiness, research focused on Indonesian regulations remains limited. This study aims to bridge this gap by adapting a design process for both the drive system and the chassis structure that adheres to or utilises equivalent alternatives to established Indonesian regulations and standards. For the drive system, GVW limitations will influence the selection of drive system components to ensure they can propel the vehicle with maximum GVW while adhering to regulations governing vehicle motion behaviour on public roads [11, 23, 24]. Similarly, the chassis structure will be designed within GVW and dimensional limitations set by Indonesian regulations. A Finite Element Method (FEM) analysis was conducted to assess the structural integrity of the chassis. Because specific regulations for the structural analysis of buses are absent, equivalent standards are adopted. These include NTE INEN 1323:2009 for deformation analysis and Ministry of Transportation Regulation number 175 of 2015 for stress analysis [25, 26]. This multi-faceted approach ensures the final bus design adheres to safety requirements and possesses the necessary structural strength.

2 Methodology

Structured methodology is crucial for designing a drive system and chassis structure that meets the desired specifications. This study adopts Dieter's design methodology, which comprises conceptual design, embodiment design, and detailed design [27]. Since detailed design focuses on documentation, this study encompasses only conceptual and embodiment design, the latter referred to as "basic design and analysis" because of its emphasis on creating a basic design and analysing the drive system and chassis structure. The flow diagram is shown in Fig. 1.

Based on Fig. 1, the design process is divided into two main processes: conceptual design and basic design and analysis. The conceptual design stage initially focuses on data collection from established sources (regulations, standards, literature, and existing products) and incorporates user experience by gathering range-anxiety data through observation and interviews with Bandung city bus operators. This comprehensive data set is then assessed to define design requirements and objectives for both the drive system and chassis structure. Subsequently, various vehicle configurations were developed and compared based on the component selection and three potential battery placement options (top, rear, and middle floor). The configuration that best met the established criteria was chosen for further development in the following design stage. In the basic design and analysis phase, the selected configuration was subjected to a more detailed design and engineering analysis. The drive system and chassis structure are meticulously evaluated to ensure they meet all established design requirements. Drive system performance is evaluated through engineering calculation, while the chassis structure undergoes Finite Element Analysis (FEA) to ensure compliance with existing regulations and standards. If any requirement remains unmet, the design is iteratively refined until all criteria are satisfied. This iterative process culminates in a finalized basic design for both the drive system and chassis structure.

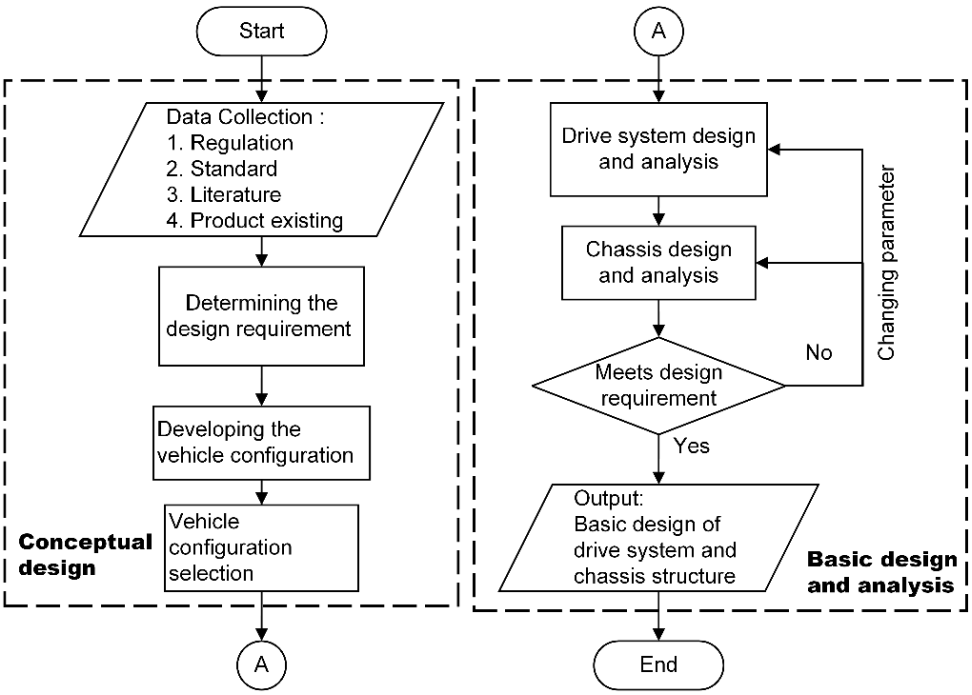

Fig. 1. Flow chart of the drive system and chassis structure design process.

3 Conceptual Design

3.1 Design Requirements

Based on Fig. 1, the initial stage of the design process involves collecting data such as regulations, standards, literature, and existing products. The collected data determines the limitations that must be met by the design of the drive system and chassis structure. The design requirements were set:

1. To fulfil the Ministry of Transportation Regulation, medium-sized bus GVW must not exceed 8,000 kg, with maximum dimensions (length × width × height) of 9 × 2.1 × 3.57 m [11]. In addition, the distance between the road surface and the bus floor at the entrance is approximately 15-30 cm to achieve a low-floor configuration to facilitate access for the elderly and people with disabilities [28].
2. The electric bus drive system design targets operation at maximum GVW on public roads with a 10% slope, achieving a top speed of 50 km/h and 1 m/s² acceleration from an idle, in accordance with regulations from the Ministry of Transportation and Ministry of Public Works and Public Housing [23, 24, 29].
3. Capable of achieving a driving range of 150 km by 80% battery Depth of Discharge (DoD) to avoid range anxiety.
4. The chassis structure satisfies structural design requirements based on the Load Resistance Factor Design (LRFD) method in NTE INEN 1323:2009, where the maximum deformation of the chassis component must not exceed 1/240 of its length [25].
5. The chassis vertical bending stiffness is in the interval 7-10 kN/mm, and torsional stiffness is in the interval 7.2-15.6 kNm/° [30].
6. The natural frequency of the chassis structure was not in the range of 0.1-1 Hz to avoid motion sickness [31].

3.2 Vehicle Configuration

After obtaining the design requirements, the next step is to create and determine the vehicle configuration. The creation of a vehicle configuration begins by selecting several basic vehicle components. Several component selection processes at the vehicle configuration creation stage.

Assuming that the vehicle's centre of gravity is in the middle, and the GVW is set to 8,000 kg, the load on each wheel axle is 4,000 kg. To ensure that the axle load capacity is higher than the actual load at the final design caused by the imprecise location of the Centre of Gravity (CoG) and the influence of dynamic loading, the load value that occurs on each shaft is increased by 25% of the estimated initial load so that each shaft can withstand a load of up to 5,000 kg.

Meanwhile, the driving range of the vehicle affects the battery capacity of the electric vehicle. The battery capacity is determined by the driving range and power consumption of the vehicle under certain conditions. Assuming the vehicle moves at a constant

speed of 50 km/hour with a road slope of 0%, it can be seen that the vehicle's traction power is 25.92 kW, assuming the drive system efficiency is 85% [12]. It is estimated that electronic components such as AC and other components consume 16 kW of power, so it is known that the total power consumed is 41.92 kW. By entering time variables based on the distance travelled and vehicle speed, the energy consumed was 125.76 kWh. It is known that the recommended Depth of Discharge (DoD) for batteries is 80% [32], and the efficiency of the electric motor is approximately 92%-97% [33]; therefore, the maximum capacity value of the battery must be greater than 170.87 kWh, which is 3 units of BMZ magnus+ battery with a capacity of 217 kWh.

For other components, such as air conditioners and wheels, the component selection process is conducted by selecting the components commonly used in medium-sized electric bus vehicles. Meanwhile, for drive system components such as electric motors and power inverters, selection is made at this stage based on the highest specifications.

Based on the description, here are some estimates of the components used as shown in Table 1 and Table 2.

Table 1. Vehicle's component data 1

Component	Amount	Dimension (mm)	Mass (kg)
Rear axle assembly	1	-	560.0
Front axle assembly	1	-	425.0
Wheels	4	Ø954 × 275	50.4
Air conditioner	1	2700 × 1630 × 195	200.0
Electric motor	1	Ø510 × 731	490.0
Power inverter	1	358 × 299 × 99	17.4
Battery	3	1356 × 800 × 371	450.0
Passenger seat	undetermined	465 × 523 × 750	6.7

Table 2. Vehicle's component data 2

Component	Amount	Dimension (mm)	Mass (kg)
Steering system	1	-	37.0 [34]
Braking system	1	-	100.0 [35]
Total without passenger seat			3381.0

Following component selection, three battery placement options (top, rear, and middle floor) observed in existing products as seen in Fig. 2 serve as reference for the development of various vehicle configurations as seen in Fig. 3. In Fig. 3, the battery placement is marked with red circles, where the first configuration battery placement is at the top, the second configuration at the middle floor and rear vehicle, and the third configuration battery placement at the rear. The battery placement influences the allocation of seating areas, standing space (marked in green), and wheelchair-accessible areas (marked in yellow) within the passenger compartment. More detailed difference between each configuration such as vehicle dimension estimation, standing area, total passenger capacity, and chassis mass estimation can be seen in Table 3.

Table 3. Vehicle configuration comparison

Criteria	First configuration	Second configuration	Third configuration
Dimension (m)	8.25 × 2.1 × 3.516	8.25 × 2.1 × 3.395	8.25 × 2.1 × 3.395
Standing area (m^2)	2.666	1.818	2.05
Passenger capacity (person)	17 (seating) + 15 (standing)	16 (seating) + 10 (standing)	15 (seating) + 12 (standing)
Chassis mass (kg)	756	769.5	737.1

The vehicle configurations will be evaluated based on four key criteria: vehicle stability, area optimization, chassis mass, and fire hazard safety. The importance of each criterion is inversely proportional to its assigned priority value (a smaller value signifies greater importance). A "worth" score will be calculated for each configuration using Eq. 1, where the sum of all priority values is used in the denominator. The configuration with the highest "worth" score will be chosen for further development in the design process.

$$worth = \frac{5 - priority\ value}{\sum priority\ value}\# \quad (1)$$

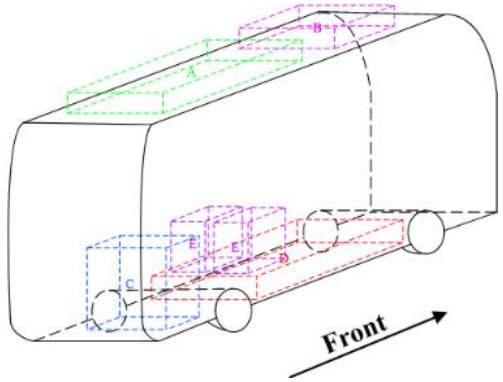

BYD 12m eBus → A&B [36]
BYD 13m eBus → A [37]
Volvo BZL electric → A [38]
Solaris Umbrino 12 Electric → A&C
Optare Versa → C [39]
Prontera Catalyst → D
Equipmake low entry → C&E [40, 41]
Equipmake low floor → C&E [40, 41]

Fig. 2. Battery placement configuration [42].

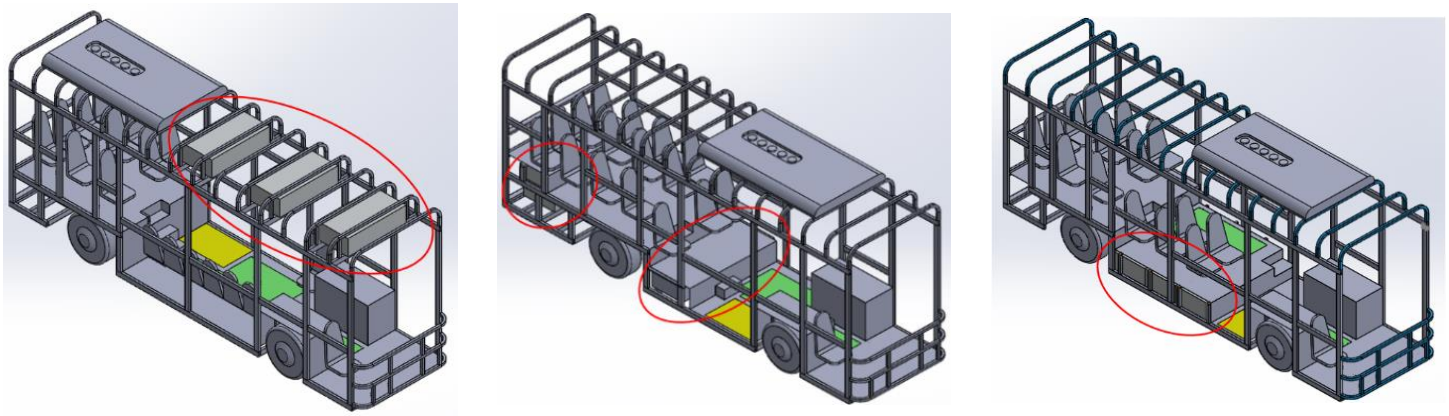

Fig. 3. (a) First configuration, (b) second configuration, (c) third configuration.

For each criterion, the configurations will be compared and assigned a rating from 1 (lowest) to 3 (highest) based on which is better or worse in that category. This rating was then multiplied by the corresponding criterion's "worth" score to obtain a weighted value for each configuration within each criterion. The configuration with the highest total score was selected for further study. As shown in Table 4, the first configuration achieved the highest total value of 2.10, which served as the foundation for the initial design, as shown in Fig. 4.

Table 4. **V**ehicle configuration selection

Category	Priority	Worth	Configuration		
			First configuration	Second configuration	Third configuration
Vehicle stability	4	0.1	0.10	0.20	0.30
Area optimization	3	0.2	0.60	0.20	0.40
Chassis mass	2	0.3	0.60	0.30	0.90
Fire hazard safety	1	0.4	0.80	0.40	0.40
Total		1	2.10	1.10	2.00

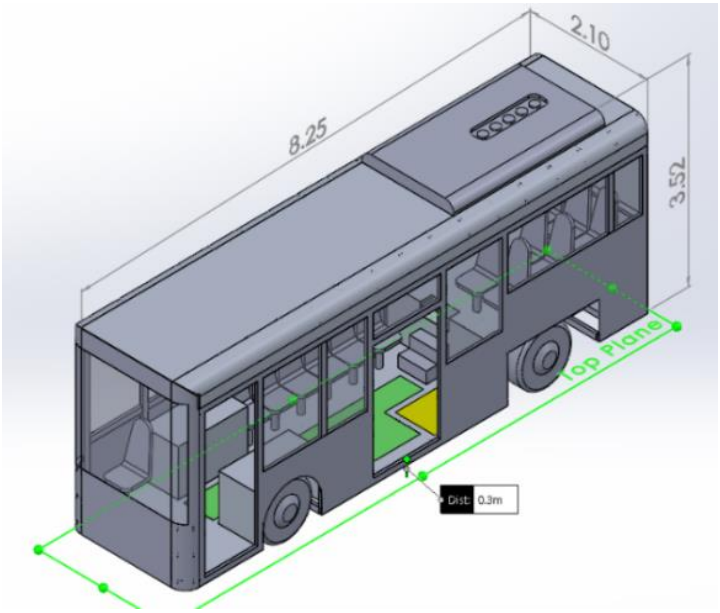

Fig. 4. 3D model of the developed medium-sized electric bus.

It can be seen in Fig. 4 that the initial design of medium-sized electric bus has estimated dimensions of 8.25 m (length) × 2.10 m (width) × 3.52 m (height), adhering to the dimension limitations set by the Ministry of Transportation (9 m × 2.1 m × 3.57 m). The bus floor height of 30 cm falls within the recommended range of 15-30 cm, ensuring easy access for passengers with disabilities and the elderly. Two entry points are provided: a central door for both regular and mobility-impaired passengers (disabled and elderly) and a front door for regular passengers. The wheelchair area is situated near the central entrance, whereas the standing passenger area is located in the central and front sections of the bus.

4 Analysis

4.1 Drive System

The drive system design process begins with determining the value of the traction force required to move the vehicle with a specific motion behaviour. A vehicle's motion behaviour is determined based on the slope of the road, vehicle speed, and acceleration capabilities [12]. Based on this description, drag forces such as gradient, rolling resistance, aerodynamics, and the vehicle's inertia will influence the traction force [12]. For more details, see Fig. 5 and its nomenclature.

Based on the design requirements, the vehicle must be able to climb a road slope up to 10%, travel up to a speed of 50 km/h, and accelerate up to 1 m/s^2. Based on this description, a matrix was created to know what condition must be fulfilled by the drive system, as shown in Table 5.

Table 5. Vehicle's motion behaviour matrix

Vehicle's motion behaviour	Road slope 10%	Road slope 0%
accelerating 1 m/s^2 from idle position	acc1grad10	acc1grad0
travel at a speed of 50 km/h	Cons50grad10	Cons50grad0

Based on Table 5, it is known that four conditions must be fulfilled. Each condition is influenced by its own drag force and its value at each condition as can be seen in Table 6.

Table 6. Vehicle's motion forces at each condition

Vehicle's motion	F_{rr} (N)	F_{ad} (N)	F_{grad} (N)	F_i (N)	F_t (N)
acc1grad10	1,015.18	0	7,809.05	8,000	16,824.23
acc1grad0	1,020.24	0	0	8,000	9,020.24
cons50grad10	1,015.18	566.12	7,809.05	0	9,390.35
cons50grad0	1,020.24	566.12	0	0	1,586.36

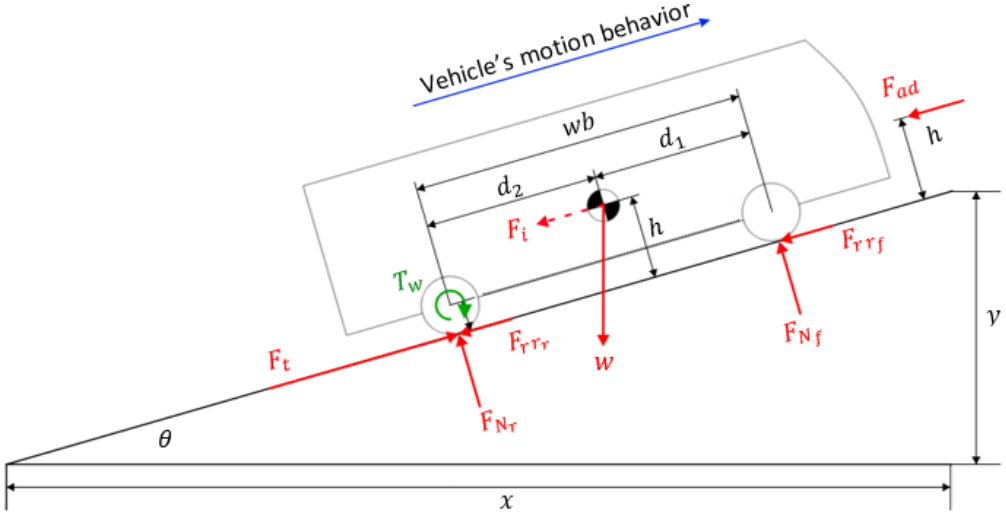

Nomenclature:
- $\boldsymbol{wb}$: Wheelbase (m)
- $\boldsymbol{d_1}$: CoG distance to front wheel (m)
- $\boldsymbol{d_2}$: CoG distance to rear wheel (m)
- $\boldsymbol{h}$: CoG distance to road surface (m)
- $\boldsymbol{F_N}$: Wheel's normal force (N)
- $\boldsymbol{F_t}$: Traction force (N)
- $\boldsymbol{T_w}$: Wheel's torque (Nm)
- $\boldsymbol{F_{ad}}$: Aerodynamics drag force (N)
- $\boldsymbol{F_{rr}}$: Rolling resistance drag force (N)
- $\boldsymbol{F_i}$: Vehicle's inertia (N)
- $\boldsymbol{\theta}$: road slope (%)
- w : Vehicle's weight (N)

Fig. 5. Free body diagram of vehicle motion behavior.

Based on the selected wheel type with an effective radius (r_d) of 0.44 m and a transmission with a final drive ratio (i_0) of 7.22 with driveline's efficiency (η_t) of 0.85 assumed [12], wheel torque (T_w), electric motor torque (T_p), and electric motor rotational speed (N_p) can be determined. Since a one-speed transmission is employed, the final drive ratio is the only applicable transmission ratio ($i_g = 1$). Using the calculated traction force and known variables, Eq. 2 and Eq. 3 were solved to determine the minimum required specifications for the electric motor. The overall calculation result is illustrated in Fig. 6.

$$T_p = \frac{T_w}{i_g i_0 \eta_t} \# \quad (2)$$

$$N_p = \frac{30 v i_g i_0}{\pi r_d} \# \quad (3)$$

Based on Fig. 6, it is known that the electric motor specifications that must be met are marked in bold. The specifications of the selected electric motor are listed in Table 7.

Table 7. Electric motor specifications and calculation result

Specifications	Value	Calculation result
Motor type	AMXE200L	
Serial number	3GLX203585-BFA	
Peak torque (Nm)	2,174	1,206.23
Peak power (kW)	569	
Peak current (A)	900	
Max speed (rpm)	4,720	
Continuous torque (Nm)	803	668.50
Continuous power (kW)	210	153.44
Continuous current (A)	308	
Nominal speed (rpm)	2,500	2,176.32

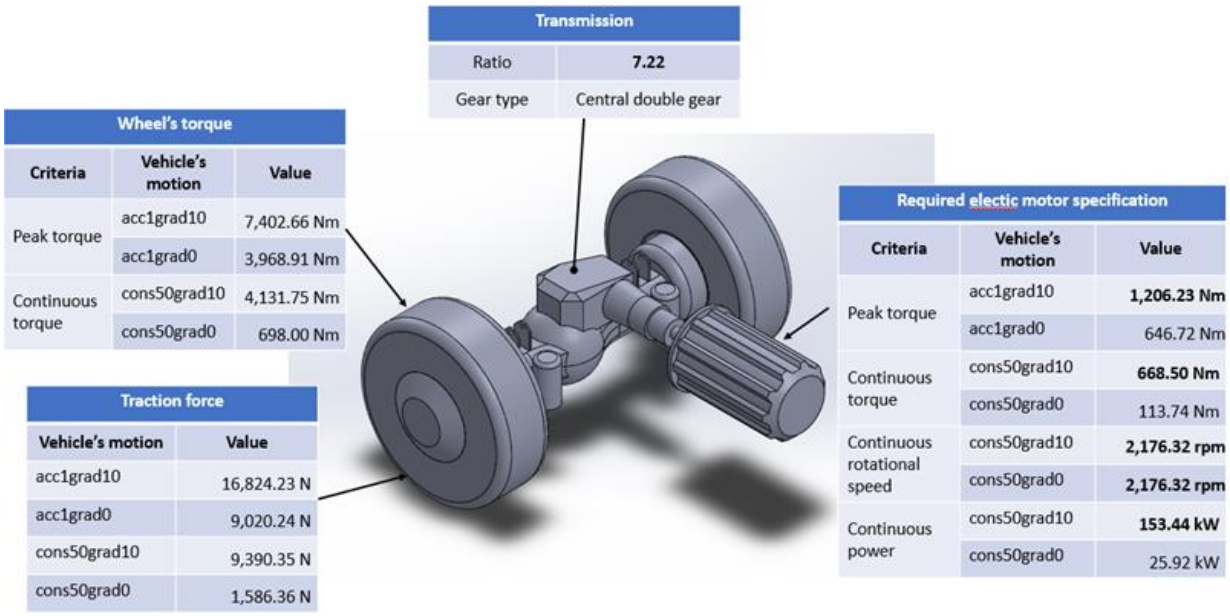

Fig. 6. Drive system calculation result.

The selected electric-motor specifications slightly exceeded the calculated results. This ensures that the chosen components meet the required performance and represent the closest match among available options in the catalogue [43]. This approach helps to prevent overdesign and potentially reduces costs.

Power inverter components are selected as an intermediary between the battery and the electric motor. The power inverter selection was determined based on the selected electric motor and battery components, as shown in Table 8.

Table 8. Power inverter selection

Category	Battery (BMZ Magnus+)	Power inverter (CM350 DX)	Electric motor (AMXE200L series)
DC voltage – operating (VDC)	566-702	200-850	-
Maximum DC voltage (VDC)	724	860	-
Motor current continuous (A)	-	500	308
Motor current peak (A)	-	800	900
Output power peak	900	440+	569

After selecting drive system components, the vehicle motion behaviour curve based on the drive system design can be seen in Fig. 7 and Fig. 8.

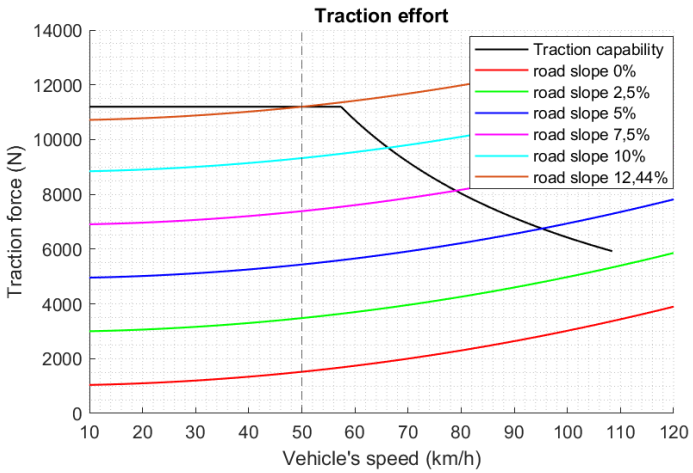

Fig. 7. Vehicle's tractive effort.

Based on Fig. 7, the vehicle's tractive capability is compared to the traction force required at specific road slopes. If the tractive capability exceeds the traction force at a given slope, the vehicle can operate effectively under those conditions. The analysis reveals that the vehicle can achieve a maximum speed of approximately 110 km/h on a 2.5% slope. Furthermore, to satisfy the design requirements, the vehicle can operate at a speed of 50 km/h on a 12.44% slope.

Fig. 8 illustrates the vehicle's acceleration capability at various road slopes, represented by coloured lines. The recommended acceleration range for passenger comfort was 1-2 m/s^2. As shown

in Fig. 8, the vehicle's actual acceleration performance falls within the range of 2.5-3 m/s^2, exceeding the recommended interval. However, this is not of a concern because the vehicle's acceleration can be adjusted through the control system to ensure a comfortable riding experience for passengers.

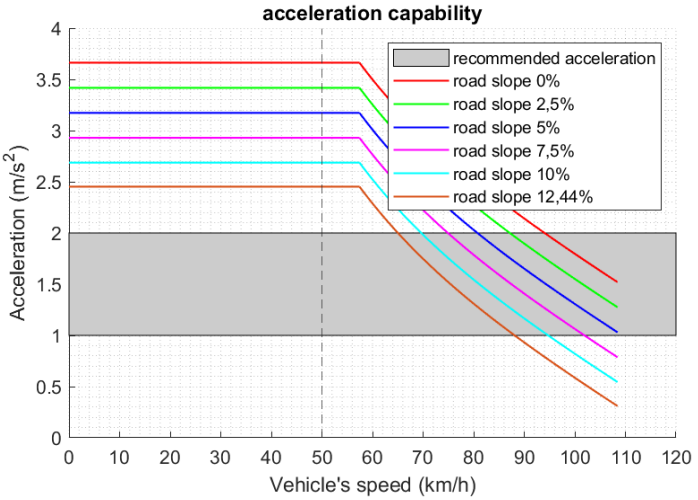

Fig. 8. Vehicle's acceleration capability.

4.2 Chassis

The geometric model of the chassis structure in each configuration is known as shown in the Fig. 3 and can be seen that the vehicle structure uses a space frame structure. The space frame structure tends to be lighter and more likely to optimize passenger cabin space and achieve a low-floor configuration than a ladder frame structure [44]. The engineering analysis process was only carried out on the selected vehicle configuration, namely, the first configuration.

4.2.1 Strength Analysis

The chassis structure strength analysis ensures that the structure does not fail during the operation of the vehicle. The strength of the chassis structure was analysed using the LRFD method referring to NTE INEN 1323:2009, in which there are diverse types of loads, such as loads due to vehicle weight, passenger weight, centrifugal force, and inertia due to acceleration and deceleration. Furthermore, these loads were multiplied by the load factor, as listed in Table 9.

Table 9. Load combination of LRFD method

LRFD case	Load combination
1	1.4M+V
2	1.2M+1.6V+0.5G
3	1.2M+0.5V+1.6G
4	1.2M+1.6F+0.8Raf
5	1.2M+0.5V+0.5F+1.3Raf
6	1.2M+1.5Ab+0.5V
7	0.9M-1.3Raf
8	0.9M+1.3Raf

Each variable in Table 9, such as M, V, G, and forth, represents the loading that occurs, with details:

1. M represents loading of bus components such as battery, electric motor, chassis structure, and forth. The value of M equals to component mass multiplied by acceleration due to gravity.
2. V represents loading of the passenger. The value of V equals to passenger mass multiplied by acceleration due to gravity.
3. G represents loading caused by the centrifugal force. The value of G equals to component or passenger mass multiplied by centrifugal acceleration, namely 2.01 m/s^2 converted from recommended cornering speed and radius [24].
4. F represents loading caused by braking force. The value of F equals to component or passenger mass multiplied by vehicle deceleration, namely 5 m/s^2 [45].
5. Ab represents loading caused by accelerating force. The value of Ab equals to component or passenger mass multiplied by vehicle acceleration, the value is equal to vehicle deceleration but with different direction [25].
6. Raf represents loading caused by aerodynamics drag. The value of Raf equals to the aerodynamics drag force at a certain condition, in this case the vehicle travels at a speed of 50 km/h.

The criteria for fulfilling the LRFD method are that no components experience deformation exceeding 1/240 of its length [25]. Moreover, the stress criteria refer to the Ministerial Regulation of the Ministry of Transportation of the Republic of Indonesia No. 175 of 2015, which states that the most critical stress in a material must not exceed 75% of the yield stress [26].

In the simulation process, loads occur by each component related to the chassis structure, represented by a point mass representing component CoG, as shown in Fig. 9.

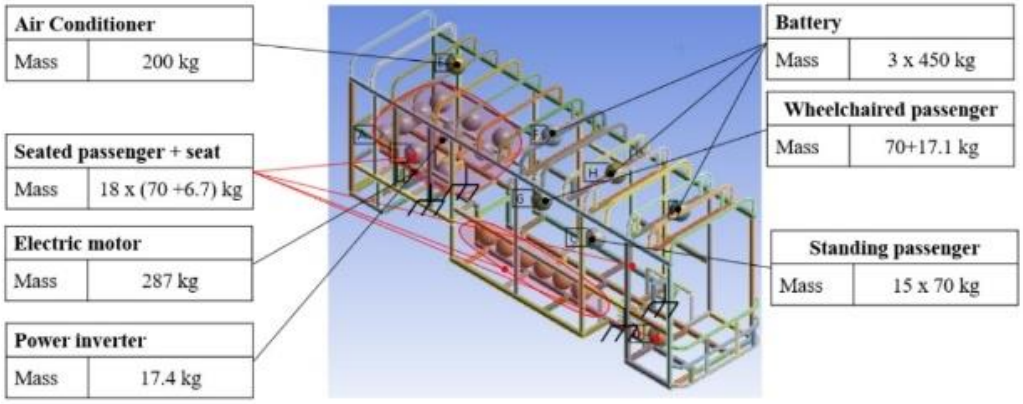

Fig. 9. Mass point designation.

After knowing the location of the loading, as shown in Fig. 9, and the magnitude of the loading are based on Table 9, a numerical simulation can be carried out with the results, as seen in Table 10.

Table 10 highlights several cases where the current chassis design fails to meet the specified stress and deformation criteria. Case 3 exceeds the allowable deformation limit of 1/240 with a critical deformation of 1/65.72. While cases 1 through 6 violate the stress criterion due to generated stresses exceeding 75% of the material's yield strength.

4.2.2 Stiffness Analysis

In addition to the structural strength, the chassis stiffness must be considered. This research analyses two types of stiffness: vertical loading and torsional stiffness.

Vertical loading stiffness analysis refers to the first case of the LRFD method because the loading occurs is pure vertical loading. So, by entering the load values and deformation that occurs as seen in Fig. 10, the stiffness value of the chassis structure can be determined by dividing the load with maximum deformation. With

a total loading of 53.90 kN and a maximum deformation of 8.67 mm, the vertical loading stiffness value is 6.22 kN/mm.

Table 10. LRFD simulation result

LRFD case	Load combination	Critical deformation ratio to its length	Critical stress compared to yield strength of material
1	1.4M+V	1/415.32	127.57%
2	1.2M+1.6V+0.5G	1/251.79	162.28%
3	1.2M+0.5V+1.6G	1/65.72	171.76%
4	1.2M+1.6F+0.8Raf	1/494.23	111.80%
5	1.2M+0.5V+0.5F+1.3Raf	1/535.12	98.38%
6	1.2M+1.5Ab+0.5V	1/359.42	96.73%
7	0.9M-1.3Raf	1/949.28	58.18%
8	0.9M+1.3Raf	1/957.31	57.57%

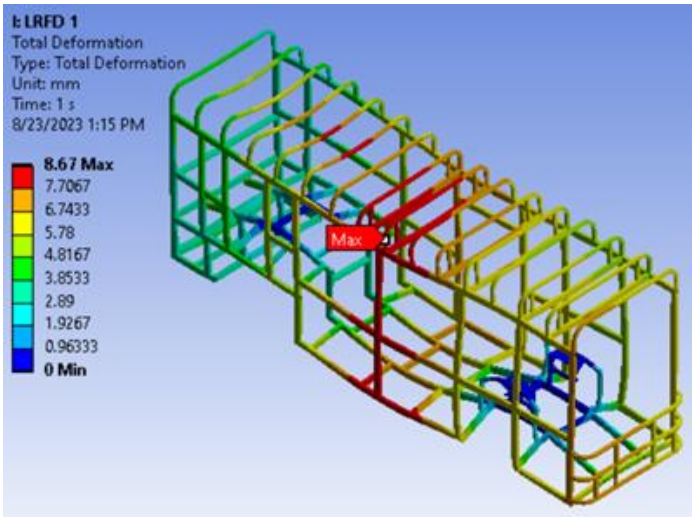

Fig. 10. Deformation simulation result of first case LRFD.

Torsional stiffness analysis is conducted by providing boundary conditions such as a fixed support at the rear suspension fulcrum, and a load is applied in the form of an opposing force at the fulcrum of the front suspension with a value of 0.25 load that occurs on each wheel owing to GVW loading with increment of 0.25 until 1 [17, 46, 47]. Loading at the front suspension fulcrum causes the chassis structure to experience torsional loading in the longitudinal direction of the vehicle. For a clearer modelling and analysis, the geometric model and boundary condition of the torsional stiffness analysis are shown in Fig. 11.

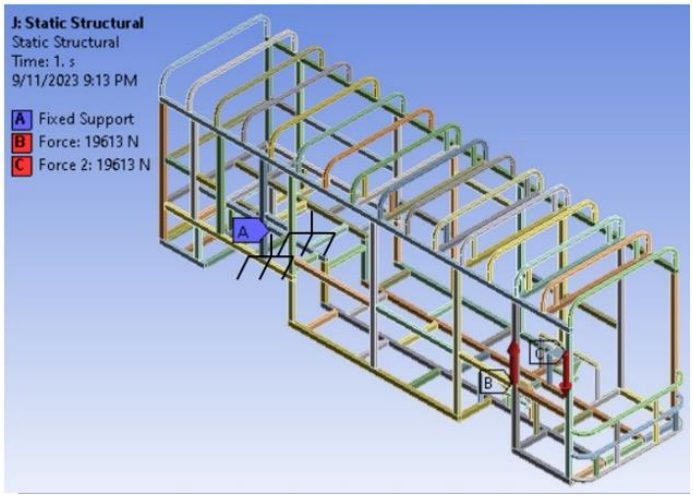

Fig. 11. Torsional stiffness model.

FEA with the geometry and boundary conditions defined in Fig. 11 provides deformation values for various cases. To quantify the angular rotation caused by torque, the deformation along the y-axis at a specific loaded fulcrum node was converted into angular rotation using Eq. 4. The resulting angular rotation values for each condition are presented in Fig. 12.

$$\theta = \arctan\left(\frac{y\ axis\ deformation}{node\ distance\ to\ rotation\ center}\right) \#\qquad (4)$$

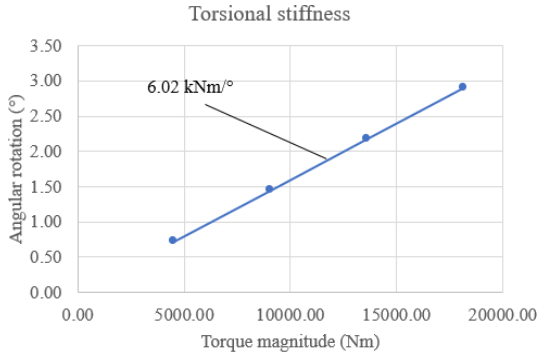

Fig. 12. Torsional stiffness result.

The stiffness analysis revealed that the chassis structure's vertical bending stiffness of 6.22 kN/mm and torsional stiffness of 6.02 kNm/° fall short of the design requirements. The design requirement specifies a vertical bending stiffness between 7-10 kN/mm and a torsional stiffness between 7.2-15.6 kNm/°.

4.2.3 Natural Frequency Analysis

Modal analysis simulations were conducted to determine the natural frequencies of the chassis structure with boundary condition refer to Fig. 13. The fixed supports were applied at the suspension fulcrums to simulate the structure's connection to the suspension system, where minimal free movement is expected. Identifying the natural frequencies ensures the chassis avoids resonance at specific frequencies, which can induce passenger motion sickness. The resulting natural frequencies are listed in Table 11.

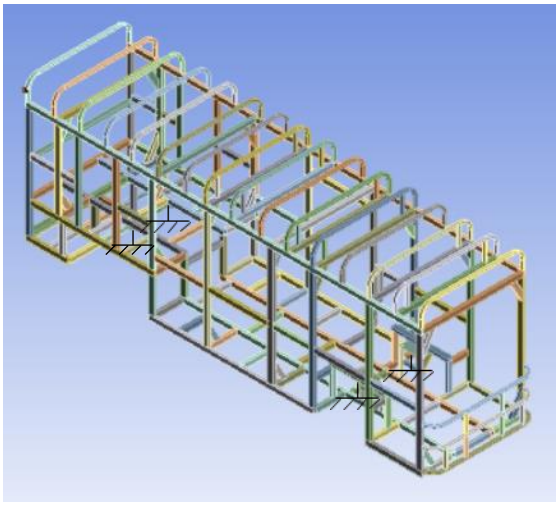

Fig. 13. Modal analysis model.

Table 11. Modal analysis result

Shape mode	Frequency (Hz)
1	4.04
2	7.92
3	10.38
4	11.85
5	13.55
6	15.36

Table 11 confirms that none of the natural frequencies of the chassis structure fall within the critical 0.1-1 Hz range across various vibration modes. This adherence to the design criteria ensures passenger comfort by avoiding resonance in this range, which can induce motion sickness.

4.2.4 Summary of Analysis

Based on the previous discussion, it is known that the chassis structure design does not meet several design requirements. Hence, an iteration must be carried out to obtain a chassis structure design that fulfils all existing design requirements. In this research, three development iterations were performed to obtain a chassis structure design that fulfilled all design requirements. The first iteration ensured the design met all requirements by replacing specific aluminium profiles with alternative specifications that satisfied all performance criteria. The second iteration prioritized manufacturability by employing a uniform material selection with optimized profile thicknesses. To ensure structural integrity despite these modifications, additional stiffeners were strategically incorporated. The third iteration targeted chassis mass reduction by utilizing thinner profiles while strategically adding structural reinforcements to maintain the required structural integrity. For more clarity, see Fig. 14. The comparative simulation results for each iteration with the same procedure as mentioned before can be seen in Table 12.

Table 12 indicates that Chassis v0 did not meet the deformation, stress, and stiffness criteria. Subsequently, development led to Chassis v1, which fulfilled all design requirements but experienced a substantial mass increase. To equalize the material, Chassis v2 was developed, resulting in a 7.6% mass increase, a 6% decrease in bending stiffness, and a 12.6% increase in torsional stiffness. To reduce the chassis mass, Chassis v3 was further developed, achieving a 4.4% mass reduction but experiencing a significant 13.6% decrease in torsional stiffness. However, the bending stiffness remained relatively unchanged, with a slight decrease of 1.8 %. Given the insignificant mass reduction and more prominent torsional stiffness change, Chassis v2 has emerged as the selected chassis design for medium-sized electric buses.

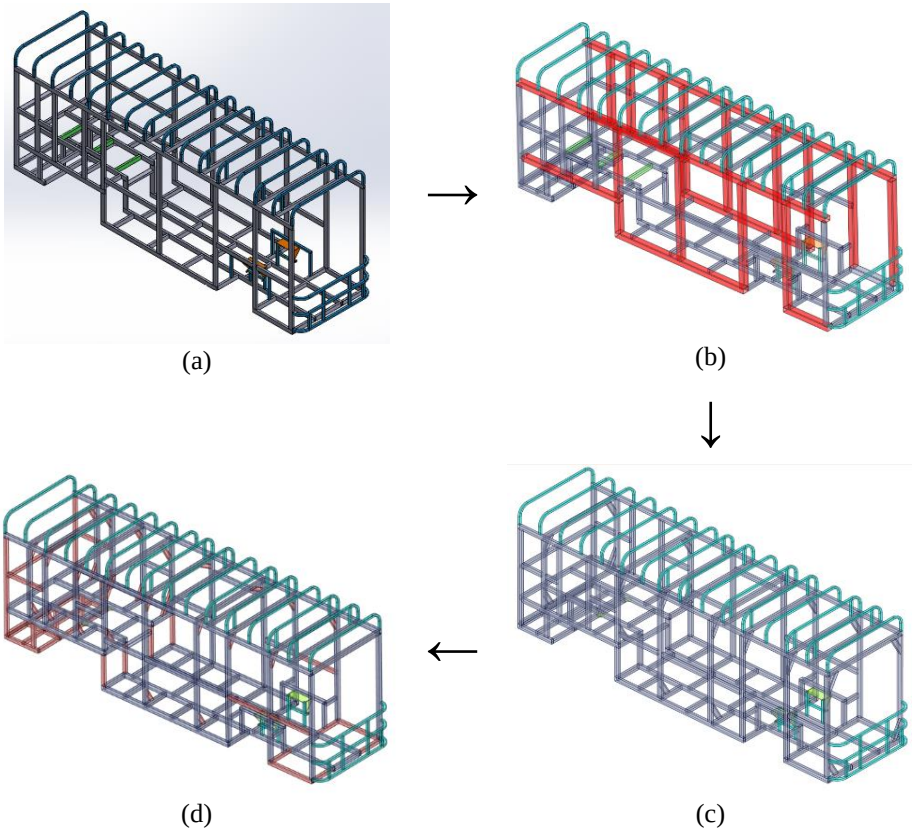

Fig. 14. (a) first model [v0], (b) first iteration [v1], (c) second iteration [v2], (d) third iteration [v3].

Table 12. Chassis structure simulation result comparison

Category	Value that must be met	chassis v0	chassis v1	chassis v2	chassis v3
Material (s)		Al 6005A T5 Al 6063 T5 Al 6060 T5 Al 5083 T5	Al 6005A T5 Al 6063 T5 Al 6060 T5 Al 5083 T5 Al 6082 T6	Al 6005A T5	Al 6005A T5
Mass (kg)	1695.34	756	924.96	994.82	951.34
Maximum deformation	≤ 1/240	1/65.72	1/289.26	1/242.69	1/302.34
Maximum stress relative	≤ 75% yield strength	171.76% yield	59.06% yield	40.22% yield	42.55% yield
Vertical load stiffness (kN/mm)	7-10	6.22	9.12	8.57	8.72
Torsional stiffness (kNm/°)	7.2-15.6	6.02	8.55	9.63	8.32
Natural frequency at first mode (Hz)	≠0.1-1	4.04	7.10	6.62	6.74

5 Conclusion

In this study, a drive system and chassis structure for a medium-sized urban electric bus comply with all design requirements. The targeted specifications included a maximum slope capability of 10 %, maximum speed of 50 km/h, acceleration of 1 m/s², and driving range of 150 km at an 80% Depth of Discharge (DoD). The chassis structure adhered to dimensional constraints of 9 × 2.1 × 3.57 m, deformation limits that a component must not exceed 1/240 of its length, critical stress limitation must not exceed 75% yield stress, specific stiffness value interval of 7-10 kN/mm for bending stiffness and 7.2-15.6 kNm/° for torsional stiffness. Additionally, the natural frequency avoided the range 0.1-1 Hz avoiding motion sickness for passenger.

Several electric bus configurations based on battery placement were evaluated. Three configurations are shortlisted: top-mounted, rear-mounted, and middle-floor-mounted batteries. These configurations were then compared across various criteria to determine the most suitable option. The configuration with the highest score is a space frame structure with top-mounted batteries and a low-floor design as seen in Fig. 4.

The selected drive system components have fulfilled all performance criteria based on design requirement. The electric motor specifications exceeded the defined values in the drive system calculation, ensuring that the drive system performance surpassed the design requirements. This translates to an impressive 12.44% grade ability, a top speed of 108.02 km/h, capability to achieve acceleration of 1-2 m/s², and an estimated range of 190.50 km.

Analysis of the initial chassis design, based on the chosen vehicle configuration, revealed limitations in meeting several design requirements. Iterative development has been used to address these shortcomings. Each iteration targeted a specific aspect: the first focused on fulfilling design requirements, the second on improving manufacturability, and the third on reducing structural mass. The second iteration, prioritizing manufacturability with uniform material, emerged as the optimal solution due to its high torsional stiffness (12.6% higher than 1st iteration and 13.6% higher than 3rd iteration) and minimal mass difference from the third iteration (4.4% difference). This final design fulfils all requirements with a critical deformation of 1/242.69, relative stress of 40.22% from yield, a vertical bending stiffness of 8.57 kN/mm, and a torsional stiffness of 9.63 kNm/°.

References

[1] P. Adhiguna. "Electrifying Indonesia's Road Transport." Institute for Energy Economics and Financial Analysis. https://ieefa.org/media/3603/download?attachment (accessed 14-12-2023, 2023).

[2] C. Sudjoko, N. Sasongko, I. Utami, and A. Maghfuri, "Utilization of electric vehicles as an energy alternative to reduce carbon emissions," in *IOP Conference Series: Earth and Environmental Science*, 2021, vol. 926, no. 1: IOP Publishing, p. 012094, doi: https://doi.org/10.1088/1755-1315/926/1/012094.

[3] Y. Noorollahi, A. Aligholian, and A. Golshanfard, "Stochastic energy modeling with consideration of electrical vehicles and renewable energy resources-A review," *Journal of energy management and technology*, vol. 4, no. 1, pp. 13-26, 2020, doi: https://doi.org/10.22109/JEMT.2019.174242.1162.

[4] D. Karina. "TransJakarta Operasikan 52 Bus Listrik, Ini Rute-rute yang Dilewati." (in Indonesian language) Kompas.tv. https://www.kompas.tv/regional/437515/transjakarta-operasikan-52-bus-listrik-ini-rute-rute-yang-dilewati?page=all (accessed 12-11-2023, 2023).

[5] I. Hidayati, "Daily Commute of Circular Migrant in Greater Jakarta: a Review: A REVIEW," *DEMOS: Journal of Demography, Ethnography and Social Transformation*, vol. 1, no. 1, pp. 14-23, 2021, doi: https://doi.org/10.30631/demos.v1i1.998.

[6] BYD Europe B.V. "BYD eBus K7." BYD Europe B.V.,. https://bydeurope.com/byd-ebus-k7 (accessed 15-06-2024, 2024).

[7] Busnex. "city-bus-e8." https://busnex.eu/city-buses/city-bus-e8/ (accessed 15-06-2024, 2024).

[8] BYD Japan. "Small electric bus J6 2.0." BYD Japan,. https://byd.co.jp/products/j6/ (accessed 15-06-2024, 2024).

[9] chinabuses. "Yutong Bus ZK6705BEVG1 E7 PLUS electric city bus." chinabuses,. https://m.chinabuses.org/product/buses/1219.html (accessed.

[10] Yutong Eurobus. "ZK6890BEVG E-vehicle." Yutong Eurobus,. https://yutongeurobus.se/wp-content/uploads/2021/06/Buss-E9.pdf (accessed.

[11] Ministry of Transportation. (2019). *Ministerial Regulation of Ministry of Transportation of the Republic Indonesia number 15 of 2019 on Organizing the Transportation of People by Public Motorized Vehicles on Routes*.

[12] M. Ehsani, Y. Gao, S. Longo, and K. M. Ebrahimi, *Modern electric, hybrid electric, and fuel cell vehicles*. CRC press, 2018.

[13] M. Ehsani, K. M. Rahman, and H. A. Toliyat, "Propulsion system design of electric and hybrid vehicles," *IEEE Transactions on industrial electronics*, vol. 44, no. 1, pp. 19-27, 1997.

[14] A. Y. Dwinanto and F. B. Muhammad, "Analisa Perbandingan Karakteristik Bodi dan Chassis pada Prototype Kendaraan Listrik," (in Indonesian language) *Rekayasa Mesin*, vol. 6, no. 2, pp. 101-105, 2015, doi: https://doi.org/10.21776/ub.jrm.2015.006.02.2.

[15] D. C. Barton and J. D. Fieldhouse, "Vehicle Structures and Materials," in *Automotive Chassis Engineering*, D. C. Barton and J. D. Fieldhouse Eds. Cham: Springer International Publishing, 2018, pp. 215-254.

[16] S. Gawande, A. Muley, and R. Yerrawar, "Optimization of torsional stiffness for heavy commercial vehicle chassis frame," *Automotive Innovation*, vol. 1, pp. 352-361, 2018.

[17] W. Afzal and R. A. Mufti, "Optimal cross-section of cross member for increased torsional and bending stiffness of ladder frame chassis," in *2019 16th International Bhurban Conference on Applied Sciences and Technology (IBCAST)*, 2019: IEEE, pp. 218-228, doi: https://doi.org/10.1109/IBCAST.2019.8667195.

[18] R. Saini, R. Jindal, S. Kumar, M. Tayyab, and R. M. Singari, "Weight Optimization and Structural Analysis of an Electric Bus Chassis Frame," *International Journal of Research in Engineering, Science and Management*, vol. 5, no. 5, pp. 7-10, 2022.

[19] K. G. Alifio, J. B. Ariatedja, and B. Sudarmanta, "Analisis Material Ringan pada Bus Body Frame Battery Electric Vehicle Bus PUI SKO ITS dengan Metode Elemen Hingga," (in Indonesian language) *Jurnal Teknik ITS*, vol. 10, no. 2, pp. E311-E318, 2021, doi: https://doi.org/10.12962/j23373539.v10i2.74306.

[20] O. Kurdi *et al.*, "Analisa Statik dan Optimasi Size Chassis Bus Medium dengan Metode Elemen Hingga," (in Indonesian language) *ROTASI*, vol. 22, no. 4, pp. 272-281, 2020, doi: https://doi.org/10.14710/rotasi.22.4.272-281.

[21] S. Wicaksono, M. Rahman, S. Mihradi, and S. Prifiharni, "Finite element analysis of bus rollover test in accordance with UN ECE R66 Standard," 2017, doi: https://doi.org/10.5614/j.eng.technol.sci.2017.49.6.7.

[22] O. Arteaga *et al.*, "Design and structural analysis of an interprovincial bus applying the LFRD method," *Materials Today: Proceedings*, vol. 27, pp. 352-358, 2020, doi: https://doi.org/10.1016/j.matpr.2019.11.114.

[23] Ministry of Transportation. (2015). *Ministerial Regulation of Ministry of Transportation of the Republic Indonesia number 111 of 2015 on Procedures for Determining Speed Limits*.

[24] Ministry of Public Works and Public Housing. (2021). *20/SE/Db/2021, Pedoman desain geometrik jalan*.

[25] INSTITUTO ECUATORIANO DE NORMALIZACIÓN, "NTE INEN 1323: 2009," *Veículos automotivos, carrocerias de ônibus. Requisitos" Quito, Equador: Instituto Equatoriano de Normalização*, pp. 2-8, 2009.

[26] Ministry of Transportation. (2015). *Ministerial Regulation of Ministry of Transportation of the Republic Indonesia number 175 of 2015 on Standard Technical Specifications for Normal Speed Trains with Self Propulsion*. [Online] Available: https://peraturan.bpk.go.id/Home/Details/103608/permenhub-no-175-tahun-2015
[27] G. E. Dieter and L. C. Schmidt, "Engineering design. The United States," ed: New York: McGraw–Hill, 2009.
[28] Ministry of Public Works and Public Housing. (2018). *02/SE/M/2018, Perencanaan Teknis Fasilitas Pejalan Kaki*.
[29] X. Karekla, K. Gkiotsalitis, and N. Tyler, "The impact of a passenger-safety-driven acceleration limit on the operation of a bus service," *Accident analysis & prevention*, vol. 148, p. 105790, 2020, doi: https://doi.org/10.1016/j.aap.2020.105790.
[30] G. Genta and L. Morello, *The automotive chassis*. Springer, 2009.
[31] B. Cheung and A. Nakashima, "A review on the effects of frequency of oscillation on motion sickness," *Defence R&D Canada Toronto Technical Report*, pp. 10-11, 2006.
[32] BMZ GROUP. "Magnus+ Latest Generation of the Commercial E-Mobility Battery." BMZ GROUP. https://bmz-group.com/images/Magnus_E-Mobility_Battery.pdf (accessed 24-09-2023, 2023).
[33] K. Dambrauskas, J. Vanagas, T. Zimnickas, A. Kalvaitis, and M. Ažubalis, "A method for efficiency determination of permanent magnet synchronous motor," *Energies*, vol. 13, no. 4, p. 1004, 2020, doi: https://doi.org/10.3390/en13041004.
[34] VSE. "VSE ELECTRONIC BUS STEERING." VSE. https://www.v-s-e.com/bussen/vse-electronic-bus-steering (accessed 2023).
[35] S. Prasetya, M. Adhitya, H. D. Budiono, and D. A. Sumarsono, "A investigation of braking system actuators for electric shuttle bus," in *E3S Web of Conferences*, 2018, vol. 67: EDP Sciences, p. 01023, doi: https://doi.org/10.1051/e3sconf/20186701023.
[36] BYD Europe. "12m eBus." BYD Europe B.V. https://bydeurope.com/pdp-bus-model-12 (accessed 18-10-2022, 2022).
[37] BYD Europe. "BYD Chassis." BYD Europe B.V. https://bydeurope.com/pdp-chassis (accessed 18-10-2022, 2022).
[38] Volvo Bus Corporation. "Volvo BZL Electric." Volvo Bus Corporation. https://www.volvobuses.com/en/city-and-intercity/chassis/volvo-bzl-electric.html (accessed 18-10-2022, 2022).
[39] Optare. "Solo and Versa EV." Optare. http://blogs.coventry.ac.uk/covid/wp-content/uploads/sites/11/2014/02/Optare-Solo-Versa-EV.pdf (accessed 18-10-2022, 2022).
[40] Equipmake. "MT17.0 LE." Equipmake. https://equipmake.co.uk/products/mt17-0le/ (accessed 18-10-2022, 2022).
[41] Equipmake. "MT17.0 LF." Equipmake. https://equipmake.co.uk/products/mt17-0-lf/ (accessed 18-10-2022, 2022).
[42] R. Bisschop, O. Willstrand, and M. Rosengren, "Handling lithium-ion batteries in electric vehicles: preventing and recovering from hazardous events," *Fire technology*, vol. 56, no. 6, pp. 2671-2694, 2020.
[43] ABB. "ABB Motors for heavy electric vehicles." ABB. https://new.abb.com/motors-generators/iec-low-voltage-motors/heavy-electric-vehicles (accessed 24-09-2023, 2023).
[44] A. Y. Dwinanto and F. B. Muhammad, "Analisa Perbandingan Karakteristik Bodi dan Chassis pada Prototype Kendaraan Listrik," (in Indonesian language) *Jurnal Rekayasa Mesin*, vol. 6, no. 2, pp. 101-105, 2015, doi: https://doi.org/10.21776/ub.jrm.2015.006.02.2.
[45] Indonesian government. (2012). *Government Regulation of Indonesia number 55 of 2012 on Vehicle*.
[46] B. Y. Wahyudi, B. Sudarmanata, and J. B. Ariatedja, "Analisa Torsional Rigidity dan Bending Stiffness pada Bus Elektrik PUI-SKO ITS Konversi ICE ke BEV dengan Variasi Cross Member," *Jurnal Teknik ITS*, vol. 10, no. 2, pp. E303-E310, 2021, doi: https://doi.org/10.12962/j23373539.v10i2.74299.
[47] A. K. Ary *et al.*, "Numerical estimation of the torsional stiffness characteristics on urban Shell Eco-Marathon (SEM) vehicle design," *Curved and Layered Structures*, vol. 8, no. 1, pp. 167-180, 2021, doi: https://doi.org/10.1515/cls-2021-0016.